HEIRARCHY OF PHOTONIC EFFECTS IN 3D PRINTED PHOTONIC STRUCTURES

Physical Sciences Final Year Project

by

Ezra Nielsen

Trinity College Dublin

2022-23

Supervised by Louise Bradley

Abstract: Using diffraction and phase grating theory, Lumerical and MATLAB simulations, 3D printed grating samples with varying dimensions were analysed. The most vibrant colours in the zeroth order occurred in structures with an aspect ratio of 0.33 (as previously discovered[1]) with the most adherence to phase grating theory occurring at an aspect ratio of 0.25. Blueshifts were observed for spectra of samples in various liquids as refractive index increased, and redshifts were observed as sample height increased (both consistent with expectations of Equation 1).

Acknowledgements: I was shown how to observe and measure the samples by Jing Qian using a microscope and an experimental setup (Figure 4). All data mentioned in this report was taken by either Jing Qian or myself and Jing Qian. All analysis based on the data for this project was done independently. Jing Qian had the samples made with specific dimensions before my project began using a Nanoscribe device which I was introduced to by Colm Delaney when a new set of samples was made. The exact dimensions of the samples were determined using AFM and SEM measuring techniques by Srikanth Kolagatla and Colm Delaney respectively. Figure 1 was created using the 3D Paint program, and Figures 2 and 3 were created by digitally removing the background of images of the two slides. Figures 1-4 were labelled using PowerPoint. The original images which were edited for Figures 2 and 3 were taken by Jing Qian. The Lumerical simulation mentioned in this report was also done by Jing Qian.

Contents

Introduction: The phenomenon which allows the presence of colour in some natural structures in the absence of any dye is referred to as structural colour. Structural colour occurs due to the interaction of light with the lattice structure of the feature itself; such as a peacock feather which innately possesses an iridescent hue. One objective of the field of photonics is to recreate these structural colours artificially. This allows for a novel approach to colour for industries such as fashion, electronics, and architecture as well as a sustainable alternative to paints and dyes.[4] Photonic structures are periodic[11] structures with values of period in the nanometre scale such that they can reflect (or diffract in the case of transmission grating) visible wavelengths of light (400-700 nm). Diffraction gratings are structures that separate a light source into a diffraction pattern of spectra according to the constructive and destructive interference of the electromagnetic waves present in the source (such that constructive interference leads to a high value of intensity at a given point represented by a light band[13] and destructive interference leads to a low intensity represented by a dark band[13]). Gratings are composed of equidistant parallel lines[12] on either a glass or metal sheet (Figure 1 shows the case of a glass sheet) which corresponds to transmission and reflection gratings respectively. The transmission gratings are printed on glass such that the light can pass through the gaps (or slits) between the parallel lines. Likewise, the reflection gratings are printed on metal such that the light is reflected by the metal in the gaps. As with structural colour, a prominent interest of photonics research is the optical effects of photonic structures. Merging the objective to artificially produce structural colour with the interest in the optical effects of photonic structures allows for examining the optical effects of photonic structures and noting the dimensions of the structure which allow it to exhibit structural colour. This is accomplished by using diffraction theory as well as phase grating theory when analysing the spectra to compare the expected results to what is observed and altering expectations accordingly. 3D printed IPL transmission grating of varying height and gap (slit) width was analysed by taking spectra at specified detector angles, photographing results, and performing MATLAB simulations based on phase grating theory. The grating samples were 3D printed onto glass slides and organized according to sample height and gap width. Figure 1 below is a digital representation of the composition of a portion of a grating sample with labelled dimensions which will be relevant to the discussion in this report.

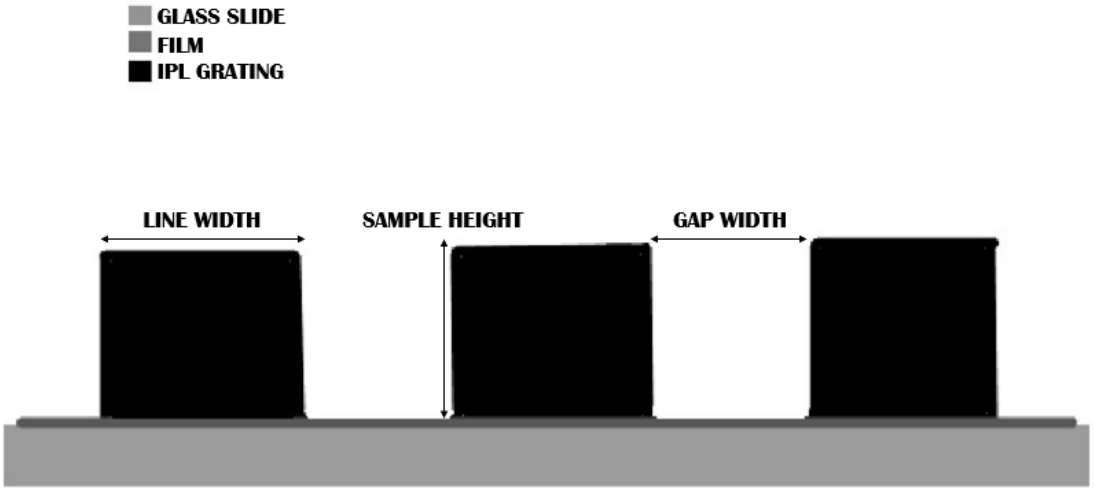

Figure 1: Grating Sample Dimension Notation

Figure 1 shows the dimensions of the grating samples which will be discussed (line width, sample height, and gap width). The legend in the top left corner is the colour-coding of the different portions of the sample slide for clarity and does not represent the colour of the slides. The portions of the sample slides are the glass slide on which film is placed and IPL grating is 3D printed over.

Two slides printed with sets of samples were analysed and referred to as Slide 1 and Slide 2 respectively. Sample maps of these slides are shown as Figures 2 and 3.

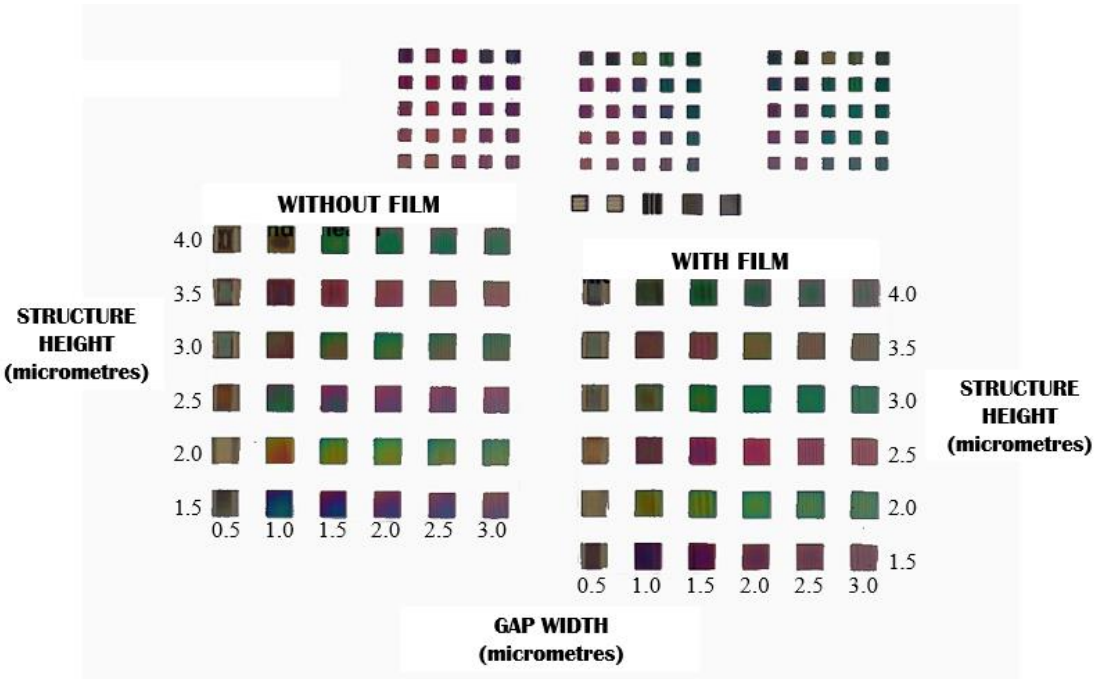

Figure 2: Sample Map of Slide 1 with Labelled Dimensions

Figure 2 is a photo of slide 1 taken at zero degrees with respect to the camera and the angle of the sample where the rest of the image was removed for clarity and simplicity. The

samples in the largest two square clusters which have structure height and gap width values beside them on the vertical and horizontal axes are the ones which were analysed for this slide. The leftmost large square cluster does not have film whereas the rightmost cluster does.

Figure 3: Sample Map of Slide 2 with Labelled Dimensions

Figure 3 is a photo of slide 2 taken at zero degrees with respect to the camera and the angle of the sample where the rest of the image was removed for clarity and simplicity. The samples in the largest two square clusters which have structure height and gap width values beside them on the vertical and horizontal axes are the ones which were analysed for this slide. The leftmost large square cluster does not have film whereas the rightmost cluster does.

In the case of slide 1, the line width (width of structures separating the gaps) was set to 1.0 micrometre. For slide 2, the line width was set to 0.5 micrometres. These dimensions are relevant in calculating the grating constant 'd' which is the distance from line centre to line centre (shown in Equation 3 as line width plus gap width). The film underneath the samples in slide 1 and 2 were 0.6 micrometres thick.

For both slides (shown as Figures 2 and 3), the naming convention to reference specific samples in this report is the sample slide number followed by the "sample height"-"gap width" in micrometres (unless specified, the samples referenced can be assumed to be those with film).

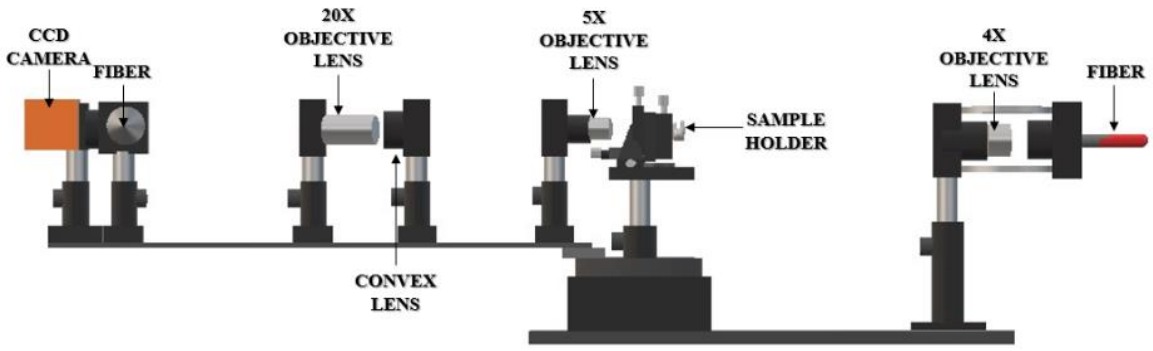

Figure 4: Experimental Setup

Figure 4 shows the experimental setup used to take data from the sample slides. The fiber connected to the white light source shone a light through the 4x objective lens which traversed the sample holder into the 5x objective lens through the 20x objective lens and into the detector (labeled as CCD camera) which was in the form of either a CCD camera for photographs or a spectrometer for spectra readings.

Using the setup in Figure 4, the white light source can be used to produce a diffraction pattern as the light passes through the grating in the sample holder. As the detector angle changes, the light visible from the detector for a given sample is at the same wavelength as the portion of the diffraction pattern expected for that angle. Since the gratings are only periodic across one axis (horizontally), the diffraction pattern also occurs horizontally. As the light passes through the slits of the grating, the electromagnetic waves interfere with one another, creating intensity peaks and troughs which correspond to the summation of the waves at a given point. Equation 2 can be used to predict what wavelength should be present at a given angle in the diffraction pattern for a sample with order number 'm' which increases and decreases from zero in integer values when moving right and left (if one is staring in the axis of the source through the sample where the light would travel).

To determine the cohesion of experimental evidence with theoretical trends graphically, a diffraction and phase grating equation will be used. For any order, Equation 1 should be used to predict the wavelengths at which intensity peaks should occur in a spectrum or set of spectra (ideally) in air or with liquid in the gaps. Equation 2 may be used to predict the angles at which different orders should occur.

$$\lambda_0 = \frac{\left(n_h h - \left((n_l t_l) + (n_a t_a)\right)\right)}{m}$$

Equation 1: Wavelength of Intensity Peak for a Phase Grating

Equation 1 is the formula for the wavelength value at which an intensity peak in the spectra of a sample should be present. In this Equation, λ_0 represents the peak wavelength value, $n_h, n_l, and\ n_a$ are the refractive indices of the hydrogel (assumed to be 1.53 for the structures in this report), liquid inside the gaps (if one is present), and air respectively. The variable h is the height of the hydrogel structure, t_l and t_a are the heights of the liquid and air in the gaps of the structures, and m is the order number (m=1, 2, 3…).

$$\boldsymbol{dsin\theta = m\lambda}$$

Equation 2: Diffraction Grating Equation

Equation 2 represents a diffraction grating with slit separation 'd', angle θ with 0 degrees being observed straight through a given slit, order number m, and wavelength λ.

$$b = \frac{l_w}{l_w + g_w} = \frac{l_w}{d}$$

Equation 3: Aspect Ratio

Equation 3 represents the aspect ratio (b) equation which is described in Knop's analysis[1] of diffraction theory for transmission phase gratings. In this equation, l_w and g_w are the line and gap width respectively, and d is the grating constant which is defined as the line plus gap width of a given grating structure.

Polymers are macromolecules (large molecules) composed by the linking of many monomers[16] (small molecules). The 3D printing process of IPL grating with a Nanoscribe device using two-photon polymerisation creates the grating structures out of crosslinked polymers; or polymers which are bonded to one another. Two-photon polymerisation creates polymers when the photoinitiator (molecule which creates free radicals when broken down[16]) absorbs energy from the focal point of a laser. The process is identified with the term "two-photon" due to the absorption of two equal wavelength photons which have the combined energy to excite the molecule into a higher energy level[15].

The use of polymers includes research in sensing, drug delivery, and the creation of artificial muscles[14]. A specific type of sensing referred to as colorimetric sensing is the colour change of a material in the presence of external stimuli. In nature, structural colour gives rise to colorimetric sensing in organisms for the purposes of camouflage or communication[17]. To attempt to mimic these biological changes experimentally (such as with photonic structures), it is preferred that the diffracted light for a given structure be within the visible range (400-700 nm) such that the change could be detected purely visually. In the case of colorimetric

sensing for the identification of solvents, the colour change may be identified as a diffraction peak shift due to change in refractive index[17] (which varies according to the liquid).

Method: The spectra were obtained using the experimental setup shown in Figure 4. Since the white light spectrum was present in these results, it was filtered out in Origin by dividing the obtained spectrum by that of the white light to obtain the spectrum of the sample itself. If the background radiation was significant, it was filtered out as well. Once normalised, the spectra were smoothed in Origin using the Loess method. When images were captured, the spectrometer was replaced with a CCD camera as shown in Figure 4. First, the zeroth order spectra were taken using the experimental setup shown in Figure 4 for both slide 1 and slide 2 by taking spectra of the individual grating samples at zero degrees. These results were plotted as contour maps of wavelength as a function of sample height by column of samples (samples of varying height from 1.5 to 4.0 micrometres with a constant gap width) which indicated where the peaks were according to the height of the samples. Secondly, the angle dependent spectra were taken for slide 2 by varying the detector or sample slide angle and taking spectra of the individual grating samples. These results were plotted on chromaticity diagrams which showed the colour saturation and wavelength of the transmitted light through the grating according to the angle. Finally, the zeroth order and angle dependent spectra were taken for slide 1 and 2 in liquid. The liquids used for measurements and analysis were water, acetone, ethanol, and IPA. Errors were calculated using the standard deviation of a given data set divided by the square root of the number of datapoints in a given set. Most Figures in this report do not include error bars (due to the average of over 3500 data points per spectrum) to allow clearer viewing of the plots. However, in the section where the Lumerical plots are compared to the obtained spectra, error bars are included since the intensity of the spectra must be used to determine the order, and in some cases although one spectrum appears above another at a given wavelength, the error of the dataset is such that the order of the spectra at that wavelength could be any of two or more spectra that are close in range.

$$E = \frac{\sigma}{\sqrt{N}}$$

Equation 4: Error Calculation

Equation 4 shows the formula for error calculation used in this report where σ represents the standard deviation of a given dataset and N represents the number of points in the dataset.

Results: Zeroth order in air

For the zeroth order spectra of slide 1 and 2 in air, Equation 1 was plotted for orders 1-4 (m=1,2,3,4) as black dashed lines on the contour plots to approximate where the peaks should be. For slide 1, as the gap width increased, the lines appeared to be closer to the centre of the peaks, which implied that as the gap width increased, the experimental data more closely matched the theoretical prediction (Equation 1). Due to this trend, the column of samples

(column 6) with the greatest gap width (3.0 micrometres) in slide 1 appeared to match the prediction most accurately.

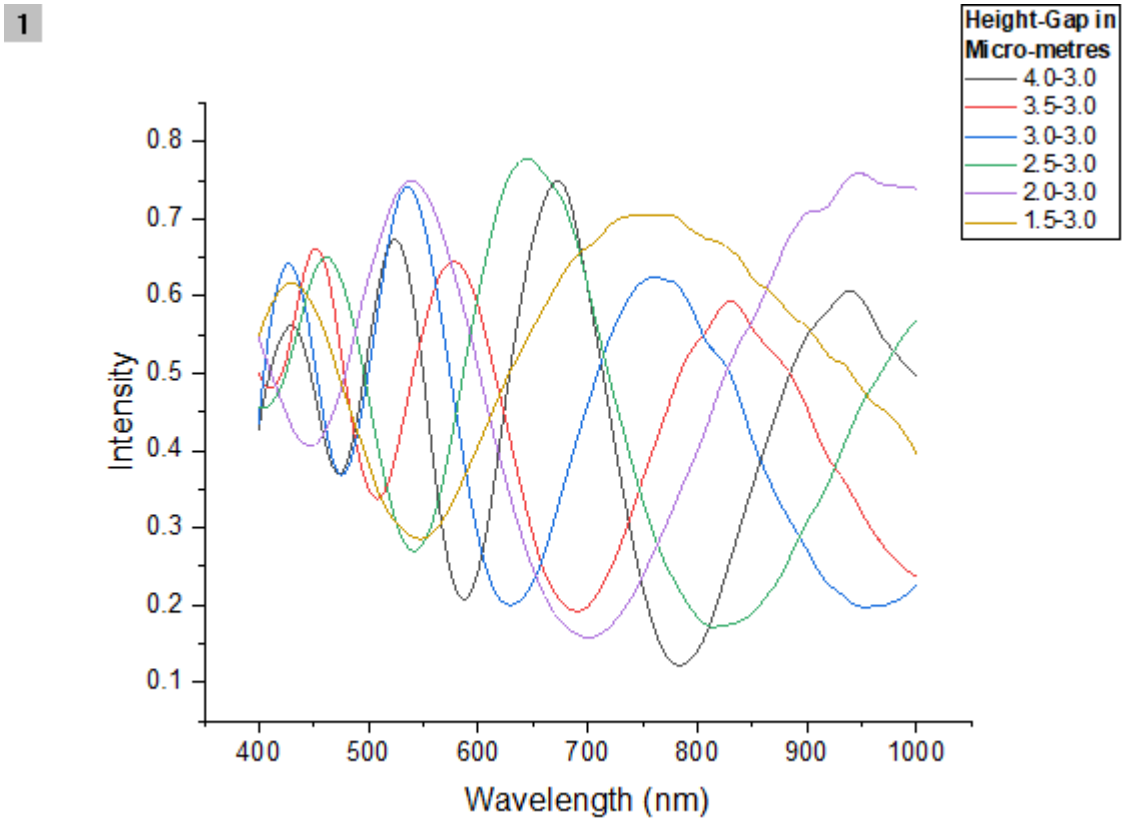

Figure 5: Sample Slide 1 Column 6 Zeroth Order Spectra in Air

Figure 5 shows the spectra of the sixth column of samples on slide 1 with intensity as a function of wavelength. These samples vary in height but possess the same gap width of 3.0 micrometres. The gap width of 3.0 micrometres is the highest of those on this sample slide and most closely demonstrates the approximation of Equation 1.

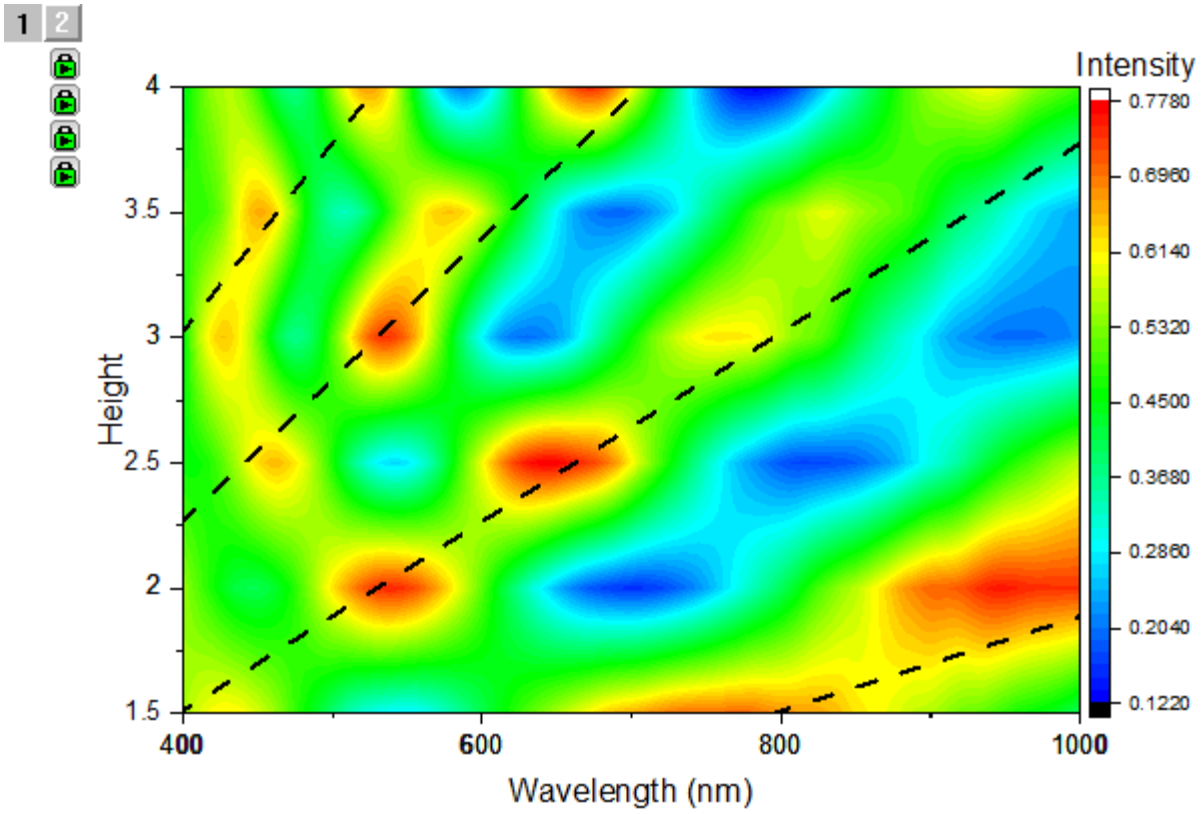

Figure 6: Sample Slide 1 Column 6 Zeroth Order Contour Map (Aspect Ratio: 0.25)

Figure 6 shows the contour map of the sixth column of samples on slide 1 with varying intensities according to a given sample spectrum. The black dashed lines are the plots of Equation 1 with orders 1-4 (m=1,2,3,4) which should predict where the peaks of the spectra should occur (the red portions of the graph are the highest intensity/peak locations). This column of samples most closely approximates the prediction of Equation 1 for slide 1.

Although column 6 of sample slide 1 most accurately matched Equation 1 (as represented by the black dashed lines), all 6 columns in slide 1 (with film) followed the general trend of Equation 1 with only slight variation in peak position to what was expected.

Analysis of Kirchhoff's scalar wave theory produced a zero-order diffraction efficiency equation which gives an expectation of the most vibrant colours present for structures with an aspect ratio of 0.5.[1] However, the results of the zeroth order diffraction of samples in slide 1 with an aspect ratio of 0.5 were the least accurate of the columns analysed. Experimentally,[1] the most vibrant colours were found in structures with aspect ratios of approximately 0.3. For the structures analysed in this report in slide 1, the final 3 rows have aspect ratios close to 0.3 and are most closely approximated by Equation 1. Therefore, for slide 1, the results obtained follow the same trend as another experiment analysing the optical effects of

transmission gratings[1] such that an aspect ratio of approximately 0.3 produces the most vibrant colours at the zeroth order.

Column Number	Aspect Ratio 'b' (Slide 1)	Aspect Ratio 'b' (Slide 2)
1	0.67	0.50
2	0.50	0.33
3	0.40	0.25
4	0.33	0.20
5	0.29	0.17
6	0.25	0.14

Table 1: Aspect Ratios for Slide 1 and 2

Table 1 shows the aspect ratios calculated from the column dimensions of slides 1 and 2 using Equation 3.

According to Table 1, despite the assumption that the sixth column of slide 1 most closely approximated the expectation of Equation 1, the fifth column is closest to the previously obtained[1] result of 0.3. At second glance, the contour map of the fifth column appears almost identical to that of the sixth column with slight deviations of peak placement.

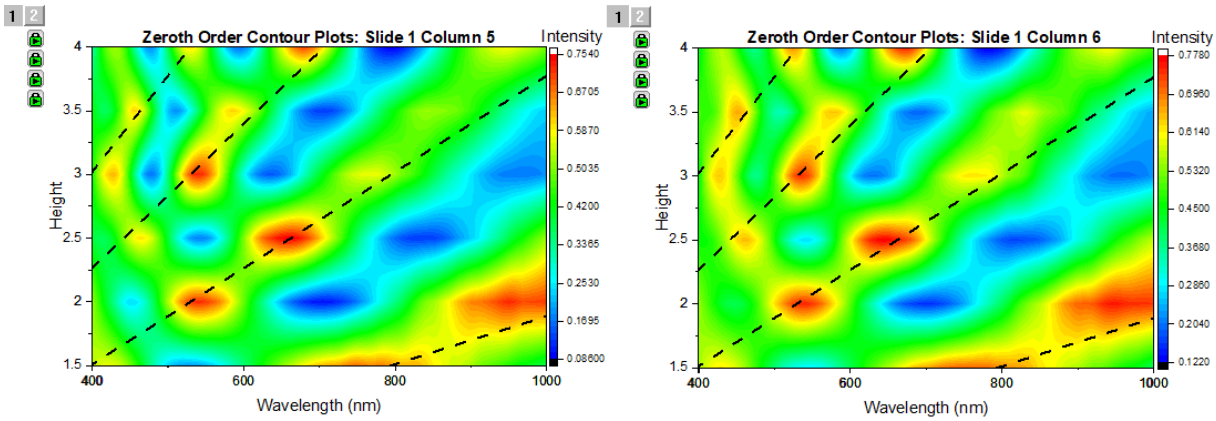

Figure 7: Zeroth Order Contour Plots of Slide 1 Columns 5 and 6 (Aspect Ratios: 0.29 and 0.25)

Figure 7 shows the contour plots of the intensity spectra of sample slide 1 columns 5 and 6 side by side such that they can be visually compared due to the expectation of a similar experiment[1].

The intensity peaks in Figure 7 for columns 5 and 6 both have closer and further intensity peak positions from the expectation when compared to one another such that the plot that is closest to expectation between the two cannot be identified in a purely visual manner.

After analysing the pattern and previously obtained expectation for the examples in slide 1, slide 2 was analysed by first simply identifying which column in slide 2 had an aspect ratio closest to 0.3. With an aspect ratio of 0.33, column 2 was identified. However, when looking at all of the contour plots, it does not appear that column 2 is the most accurately described by the expectation (Equation 1) as there are 4 visible peaks on the contour map for column 2 and the expectation lines only pass through one of them. Columns 3 and 4 appeared to be closest to expectation since the lines either passed through or appeared between (in the case of multiple small peaks close to one another) the intensity peaks.

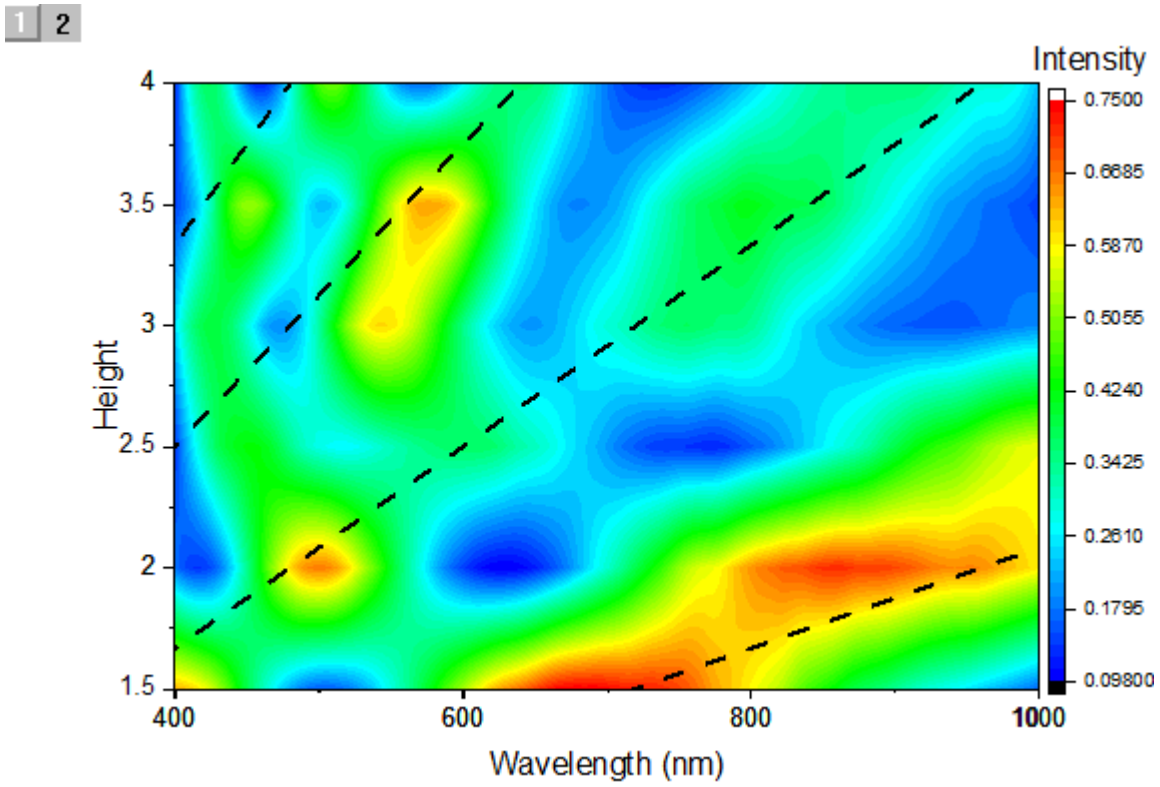

Figure 8: Sample Side 2 Column 3 Zeroth Order Contour Map (Aspect Ratio: 0.25)

Figure 8 shows the contour map of the spectra of the samples in sample slide 2 column 3 (in air) all of which have a gap width of 1.5 micrometres. The black dashed lines represent the locations of expected peaks for orders 1-4 (m=1,2,3,4) calculated using Equation 1.

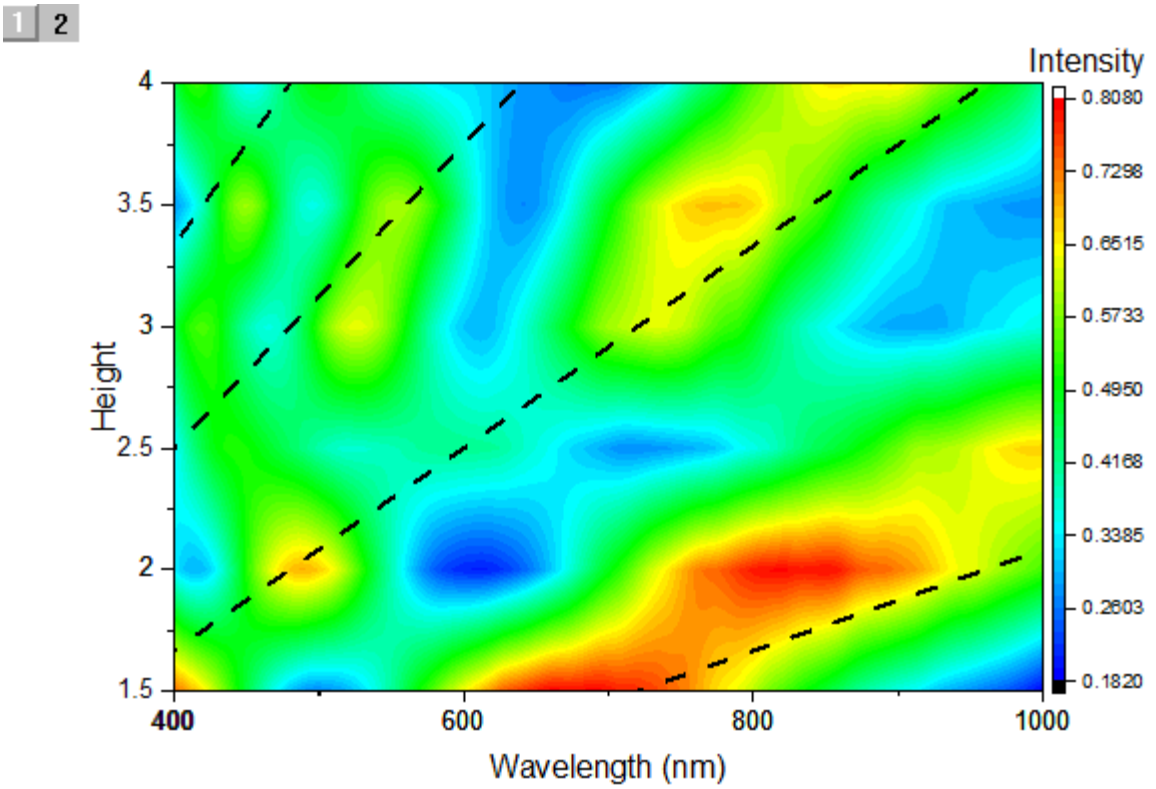

Figure 9: Sample Side 2 Column 4 Zeroth Order Contour Map (Aspect Ratio: 0.20)

Figure 8 shows the contour map of the spectra of the samples in sample slide 2 column 3 (in air) all of which have a gap width of 2.0 micrometres. The black dashed lines represent the locations of expected peaks for orders 1-4 (m=1,2,3,4) calculated using Equation 1.

Chromaticity diagrams and angle dependent measurements

Since the first column of samples in slide 1 were broken on either side, slide 2 was used for the angle dependent measurements. According to aspect ratio, column 2 of slide 2 (gap width: 1.0, aspect ratio: 0.33) was expected to have the most vibrant/saturated colours (evidenced from a past experiment[1]), and according to the contour plots, columns 3 and 4 (gap widths: 1.5, 2.0, aspect ratios: 0.25, 0.20) showed the most intense peaks closer to the expected locations according to Equation 1. The chromaticity plot of the second column of slide 2 at the zeroth shows the most saturated colours as expected in Figure 10.

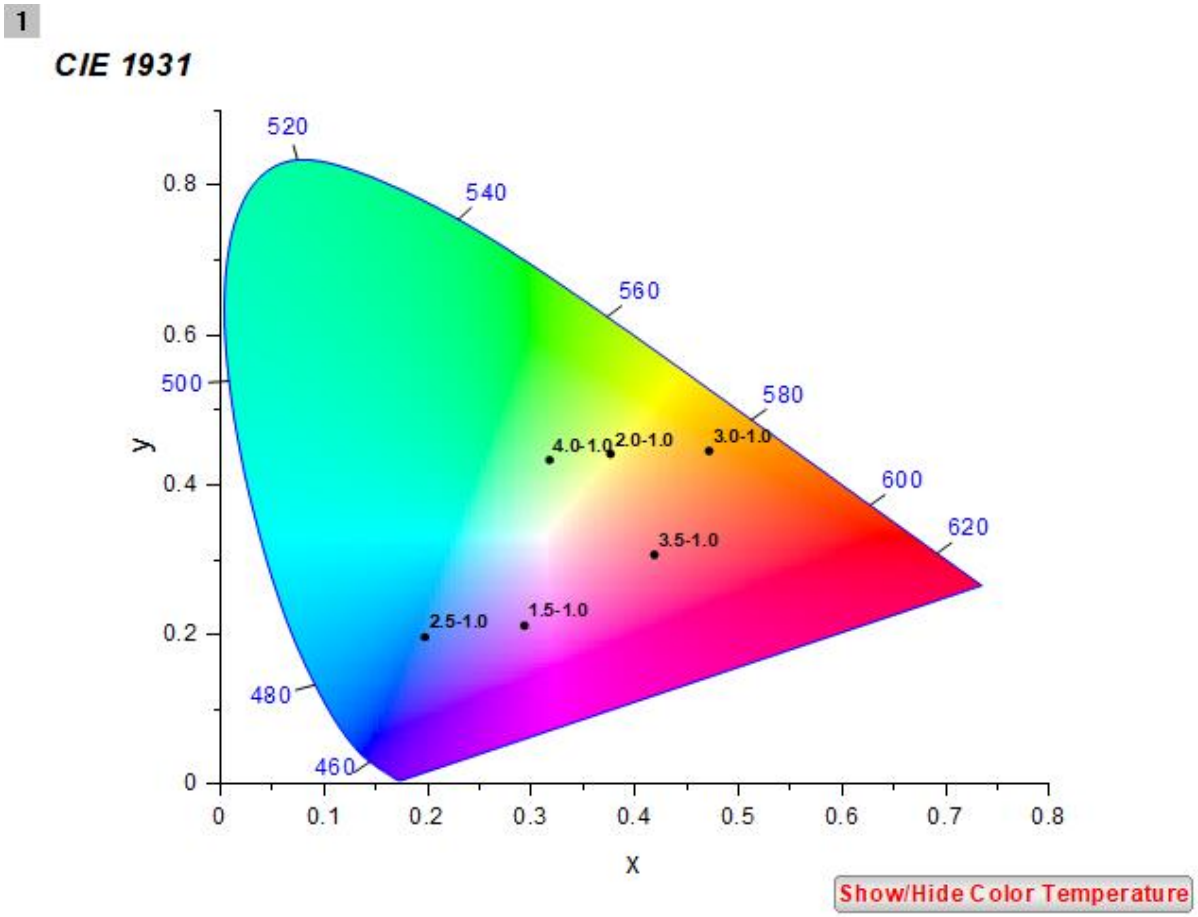

Figure 10: Sample Slide 2 Column 2 Chromaticity Diagram (Aspect Ratio: 0.33)

Figure 10 shows a chromaticity plot indicating the colour present at the zeroth order for the samples in slide 2 column 2 (shown as (sample height)-(gap width) on the plot). The distance of the points from the white centre represents the saturation of the colours such that if the points were at the centre, it would represent low saturation.

For slide 1, column 1 (aspect ratio: 0.29) was expected to have the most colour saturation at the zeroth order (evidenced from a past experiment[1]). However, the samples in column 4 of slide 1 appeared distinctively more saturated. With an aspect ratio of 0.33 (the same as that for slide 2), this may suggest that at the zeroth order, an aspect ratio of 0.33 leads to more vibrant/saturated colours than the previously determined value of 0.3.

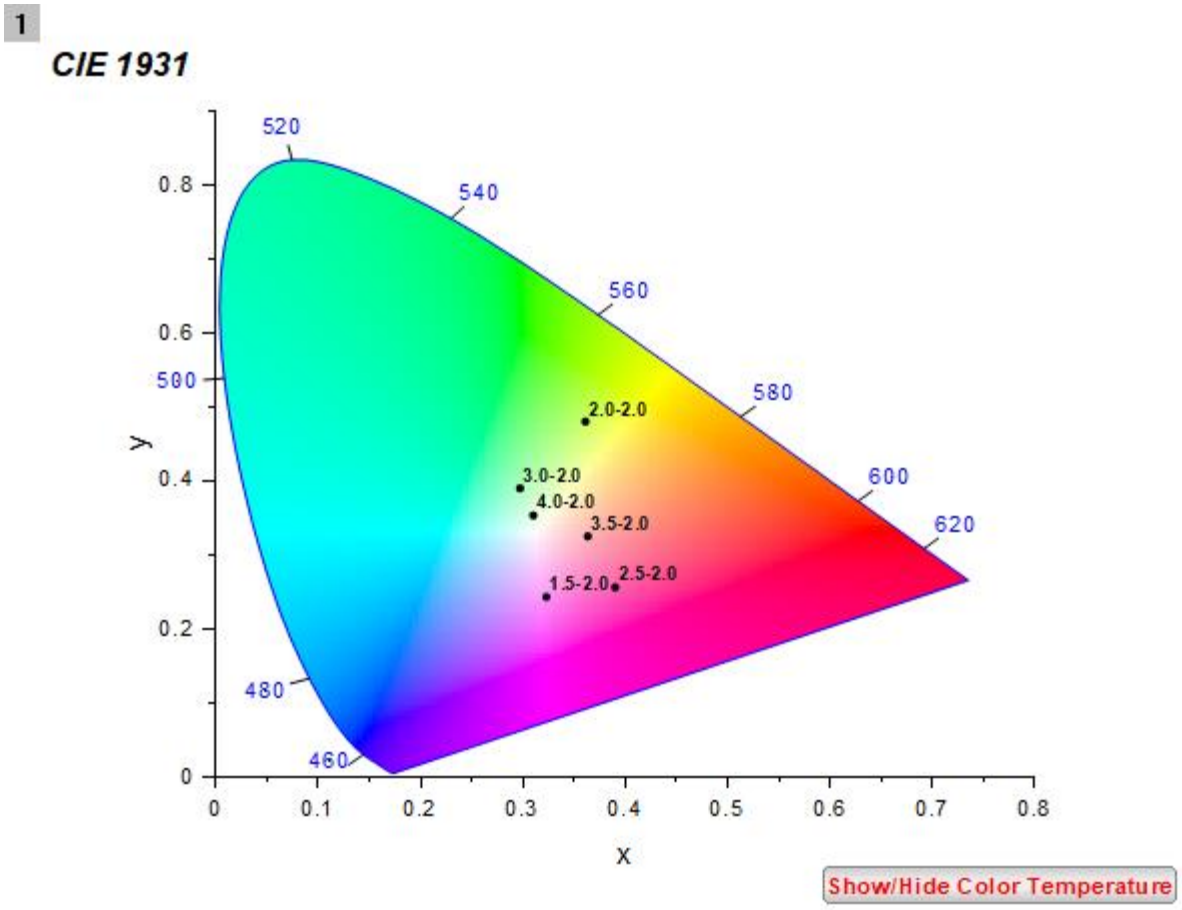

Figure 11: Sample Slide 1 Column 4 Chromaticity Diagram (Aspect Ratio: 0.33)

Figure 11 shows a chromaticity plot indicating the colour present at the zeroth order for the samples in slide 1 column 4 (shown as points with (sample height)-(gap width) on the plot). The distance of the points from the white centre represents the saturation of the colours such that if the points were at the centre, it would represent no saturation.

Although slide 1 column 4 and slide 2 column 2 have the same aspect ratio, the saturation of slide 2 column 2 is far greater than that of slide 1 column 4. The linewidth of slide 2 is 0.5 micrometres whereas the linewidth of slide 1 is 1.0 micrometre. However, when sample 2.0-2.0 on slide 1 was measured using AFM, the centre to centre (line centre to line centre) distance was found to be 2.93 micrometres as opposed to 3.0. When sample 1.5-1.0 of slide 2 was measured using AFM, the centre to centre distance was found to be 1.54 as opposed to 1.5 micrometres. Recalculating the aspect ratio based on this information gives slide 1 column 4 an aspect ratio of 0.34 and slide 2 column 2 an aspect ratio of 0.32. Therefore, although the intended aspect ratios were equivalent, the column (slide 2 column 2) with the aspect ratio closest to 0.3 possesses the most saturated colours as expected and is therefore consistent with previously obtained predictions[1].

Sample 1.5-1.5 (from slide 2) showed the most vibrant/saturated colours at high angles (measured from 0 to 25 degrees).

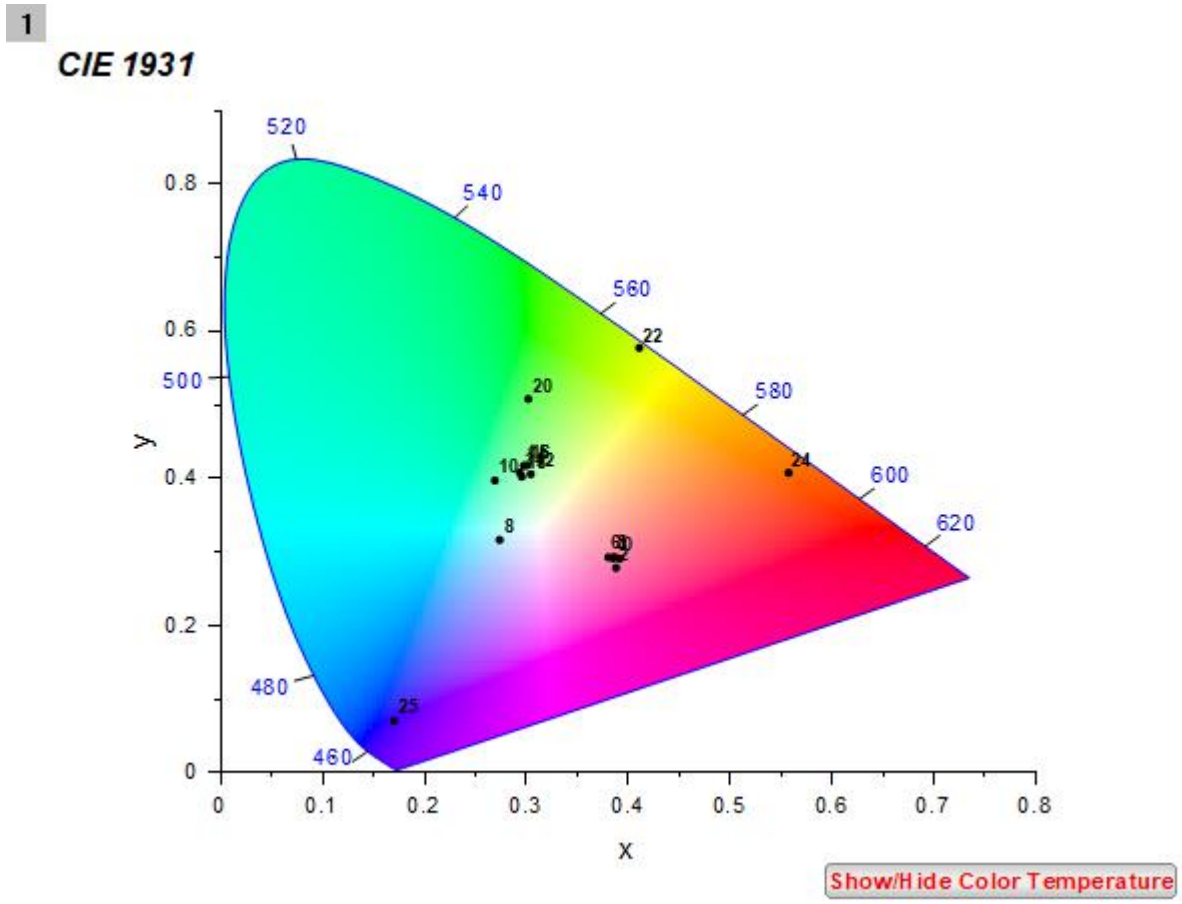

Figure 12: Slide 2 Sample 1.5-1.5 Angle-Dependent Chromaticity Diagram (0-25 Degrees, Aspect Ratio: 0.25)

Figure 12 shows a chromaticity diagram of sample 1.5-1.5 (height-gap) from slide 2 at angles ranging from 0 to 25 degrees. One may note that the saturation is greatest at the highest angles (20, 22, 24, 25).

Since sample 1.5-1.5 of slide 2 shows such vibrant colours at different angles, structures with the same dimensions could be used to reveal patterns at high angles for artistic or security purposes (such as a pattern printed onto a photo ID or credit card to verify its validity and make illegal replication more difficult).

Lumerical simulations of angle dependent measurements compared to experimental results: Slide 1 sample 2.5-2.0 (linewidth: 1.0, aspect ratio: 0.33)

Results from a Lumerical simulation were compared to a sample with the same dimensions to identify whether the experimental results would match what was obtained in the simulation. The simulation was performed for wavelengths 400, 450, 500, 550, 600, 650, 700, 750, 800, 850, and 900 nm. The analysis of experimental data was performed for the visual range of

the spectrum (400-700 nm).

(Intensity)	400 nm	450 nm	500 nm	550 nm	600 nm	650 nm	700 nm
Lowest	10	20	20	20	20	20	20
Median	20	10	10	0	10	10	10
Highest	0	0	0	10	0	0	0
Agreement (Order)	Agrees	Agrees (Error bars)	Does not agree	Does not agree	Agrees	Agrees	Agrees

Table 2: Experimental Data Compared with Lumerical Simulation for Sample 2.5-2.0 (Slide 1)

Table 2 shows the order of intensity plots from lowest to highest for the given angles. This order is compared to the Lumerical simulation relative intensity at angles 0, 10, and 20 degrees. If the order is the same, 'Agrees' is in the Agreement row for a given wavelength. If the order is not the same but error bars could compensate, leading to the expected order, 'Agrees (Error bars)' is in the Agreement row for a given wavelength. If the order is not the same and error bars could not compensate, 'Does not agree' is in the Agreement row for a given wavelength. The numbers '10', '0', and '20' represent an angle in degrees at which the given spectrum was taken.

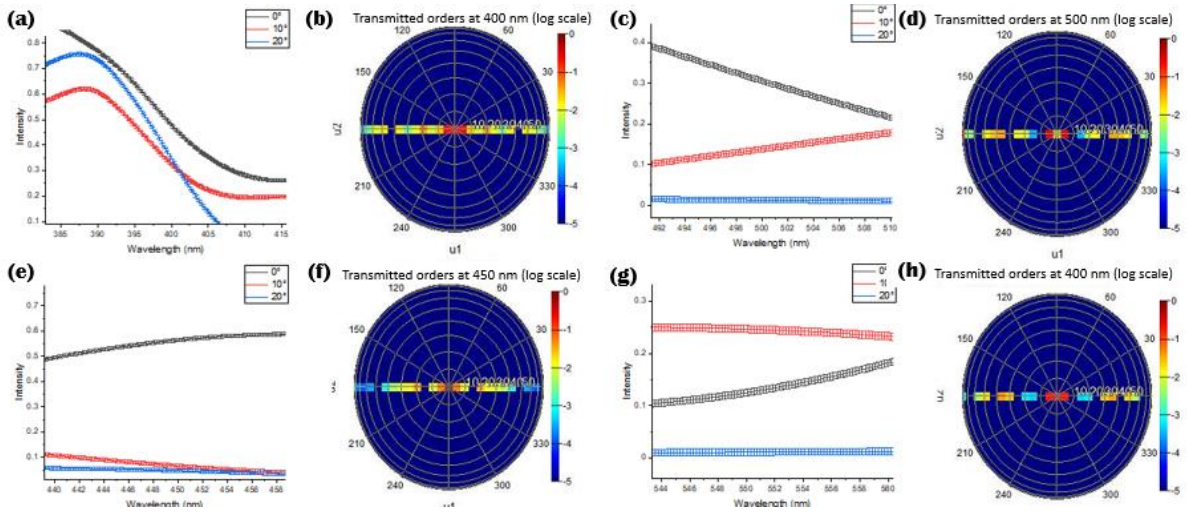

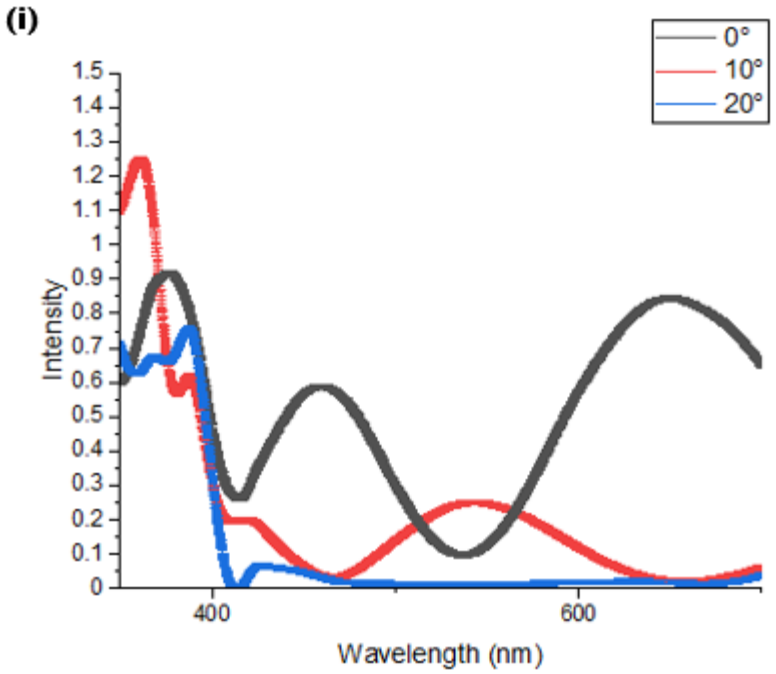

Figure 13: Experimental Data Compared with Lumerical Simulations for Sample 2.5-2.0 (From Slide 1)

Figure 13 shows the spectra for sample 2.5-2.0 at 0, 10, and 20 degrees. The full plot with error bars is Figure 13(i). The plots ((a), (c), (e), and (g)) are zoomed in to 400, 500, 450, and 550 nm respectively such that the order of the intensity of the spectra at angles 0, 10, and 20 degrees can be compared to the intensity found from Lumerical simulations ((b), (d), (f), and (h) polar plots). Plots (b), (d), (f), and (h) represent the diffraction pattern of the sample for different wavelengths. For plots (b), (d), (f), and (h), light intensity is marked on the polar plots such that black/red represents the highest intensities and blue represents the lowest.

The intensities found in the 0, 10, and 20 degree spectra for 400, 450, 600, 650, and 700 nm were in the same order as the expected intensities from the Lumerical simulations. However, the intensities found in the 0, 10, and 20 degree spectra for 500 and 550 nm were not in the same order as the experimental data. This inconsistency could be due to error in calculation/normalisation of the experimental data performed for this analysis since the spectra intensity should be as predicted by Lumerical for this sample (also since most of the spectra analysed in this report have the same intensity trends as the Lumerical data).

Samples in Liquid: Spectra

When placing the samples in liquid, the diffraction peak in the sample spectra is expected to change according to the liquid's refractive index[17] (as described in the Introduction section

of this report). The exact change in diffraction peak to be expected according to sample dimensions and liquid used may be predicted using Equation 1.

The liquids used for this portion of the report were water, acetone, ethanol, and IPA with refractive indices (as used in calculations) of 1.333, 1.3589, 1.3614, and 1.3772 respectively[19,18]. For the zeroth order (measured at 0 degrees), Equation 1 may be used to predict the expected shift in peak wavelength for each liquid and sample. As a general trend, as refractive index increases, peak location decreases, so a blueshift (shift to the left side of the spectrum) is expected in all liquid spectra as the refractive index of the liquid increases. For Slide 1 sample 4.0-1.5, the peak wavelengths at the zeroth order were first calculated based on the assumption that the height of the liquid is equal to the height of the structure. This assumption makes the simplification that the liquid fills up all of the gaps in the structures completely and is referred to in this report as Case 1. For Case 2, the assumption is made that the height of the liquid is 0.75 % of the height of the structure, and air takes up the remaining 25 %. The calculations for Case 1 resulted in values slightly higher than the experimentally obtained values (plotted on the spectra in Figure 15).

Figure 14: Assumptions Made in Peak Wavelength Calculations for Samples in Liquid

Figure 14 shows the air and water height (t_a and t_w respectively) which were assumed according to two different potential cases to calculate the expected peak wavelength from Equation 1. Case 1 assumes that the height of the liquid is equal to the height of the structure and therefore the liquid takes up all of the gap room in any given grating structure submerged in a liquid. Case 2 assumes that the height of the liquid is 75% of the height of the structure, which implies that the remaining 25% is air.

The calculations for Case 2 showed even higher wavelength values than for Case 1 which implies that decreasing the assumed height of the liquid in the gaps of a sample allows for the theoretical prediction to be even further from what was obtained in the experimental data. Therefore, one can assume that the more accurate prediction is Case 1, and since the height of the liquid in the gaps cannot be greater than the height of the sample due to the second glass

slide attached to the top of the sample slide, one must take Case 1 as the most accurate prediction possible under these conditions.

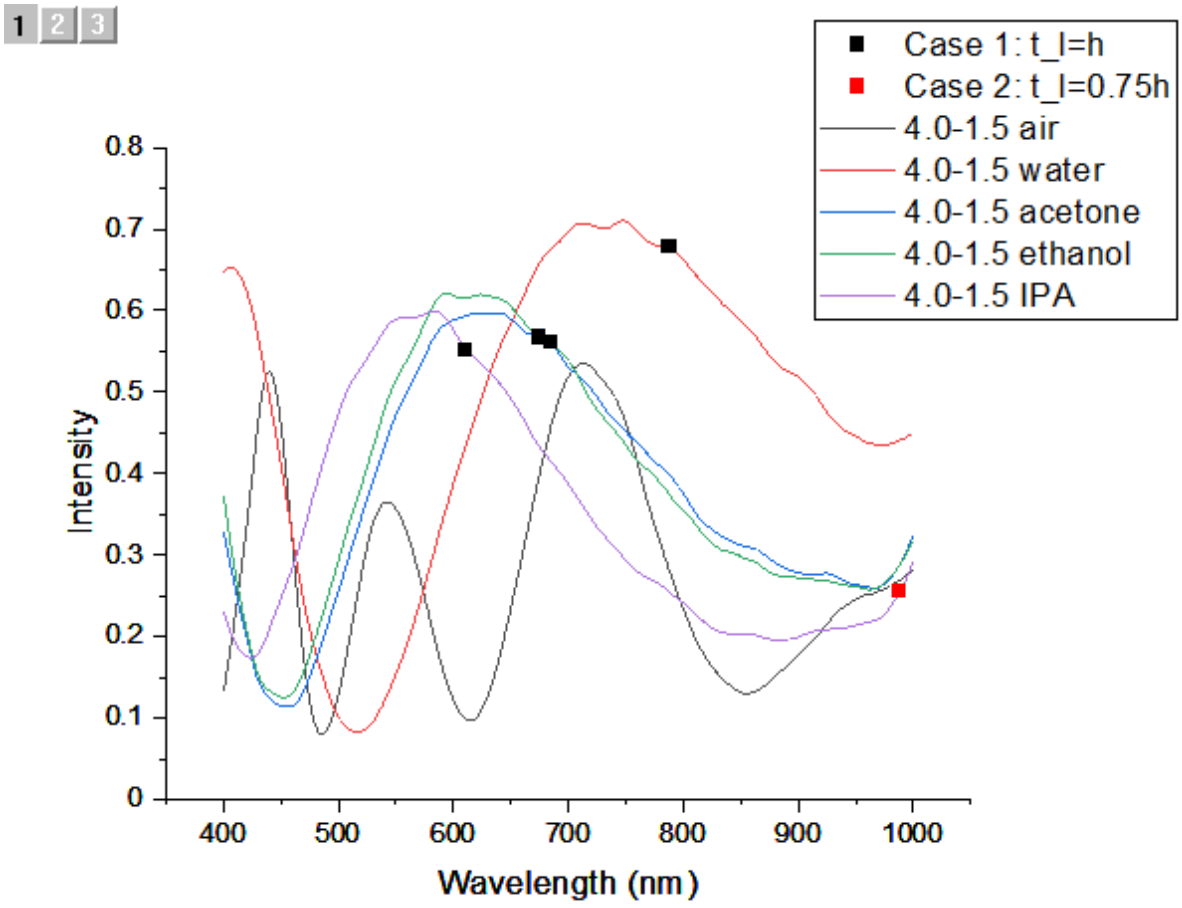

Figure 15: Case 1 and 2 Over Spectra of Sample 4.0-1.5 in Air, Water, Acetone, Ethanol, and IPA

Figure 15 shows the spectrum of light passing through the slide 1 sample 4.0-1.5 (height-gap). The peak locations decrease in wavelength as the refractive index of the liquid (or air) increases as expected. This is also the case for all other samples analysed. The peak wavelength calculations in two possible scenarios (described in Figure 14) referred to as Case 1 and Case 2 are plotted as points over the spectra.

As shown in Figure 15, Case 1 is slightly shifted to higher wavelength values with respect to the actual obtained peaks. However, Case 2 is so shifted that only the final (IPA) peak is visible over the range plotted (no expected peak values are visible for air due to the high value of the first peak past 2000 nm). Therefore, Case 1 is the more accurate assumption. Case 1 and 2 were calculated for samples of all heights and liquids (air included) in this report for reference (given in Table 3).

Structure Height (μm)	λ_0 (nm) In air	λ_0 (nm) In water	λ_0 (nm) In acetone	λ_0 (nm) In ethanol	λ_0 (nm) In IPA
	Case: 1 & 2	Case: 1, 2	Case: 1, 2	Case: 1, 2	Case: 1, 2
1.5	795	295.5, 420.4	256.7, 391.2	252.9, 388.4	229.2, 370.7
2.0	1060	394, 560.5	342.2, 521.7	337.2, 517.9	305.6, 494.2
2.5	1325	492.5, 700.6	427.8, 652.1	421.5, 647.4	382, 617.8
3.0	1590	591, 840.8	513.3, 782.5	505.8, 776.9	458.4, 741.3
3.5	1855	689.5, 980.9	598.9, 912.9	590.1, 906.3	534.8, 864.9
4.0	2120	788, 1121	684.4, 1043	674.4, 1036	611.2, 988.4

Table 3: Expected Peak Wavelength of Samples in Liquid (and Air)

Table 3 shows the calculated peak wavelength values with assumptions as described in Figure 14 as Case 1 and Case 2. The values for Case 1 were higher than what was obtained experimentally, so Case 2 was used in calculations in attempt to produce more accurate results. Case 2 resulted in even higher/more inaccurate predictions.

As expected, there was a blueshift in all samples as the refractive index of the liquid the sample was immersed in increased. This result implies that samples such as these could be used along with a spectrometer (or the naked eye depending on the intensity of the colour change) as a colorimetric sensor to identify the refractive index of a liquid based on the diffracted peak position of a known sample in that liquid compared to the peak position obtained using a liquid with a known refractive index.

Samples in Liquid: MATLAB Simulations

MATLAB simulations were performed on the samples in various liquids to determine the expected peaks of each structure. These were plotted as line and symbol graphs of peak wavelength as a function of the liquid refractive index.

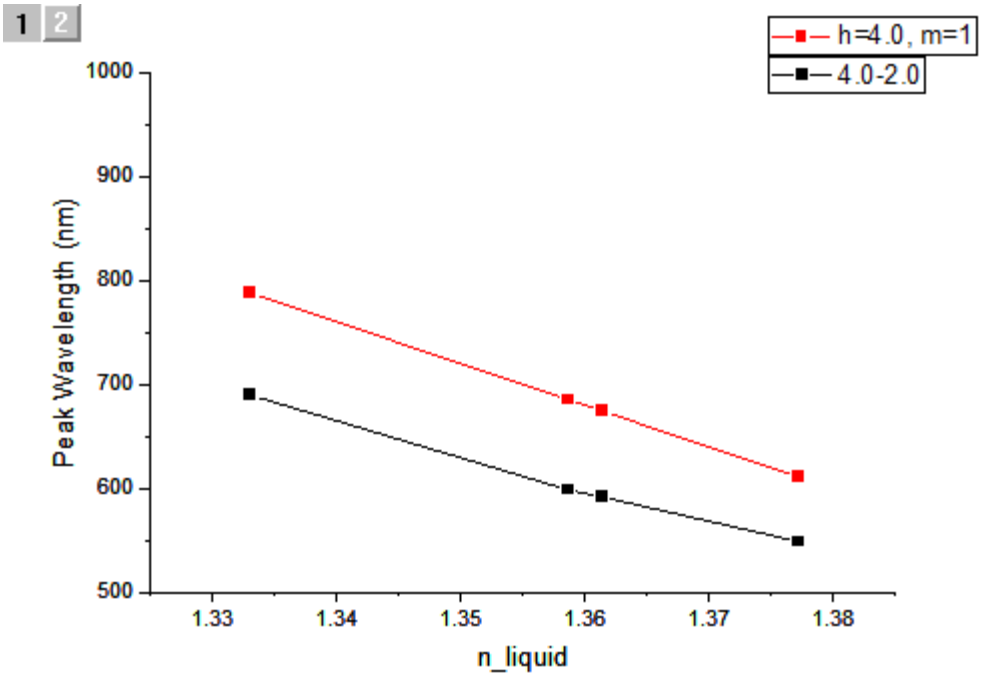

Figure 16: Sample 4.0-2.0 MATLAB Peak Wavelength Simulation (Red) with Experimental Data (Black)

Figure 16 shows a plot of peak wavelength as a function of the refractive index of the liquid which sample 4.0-2.0 is immersed in. The red plot is the MATLAB simulation data, and the black plot is the experimental data. The variable 'm' in the legend represents the order number with respect to the order of a given diffracted spectrum.

In Figure 16, the experimental data follows the trend of the MATLAB simulation as expected with peak wavelength always increasing as refractive index decreases.

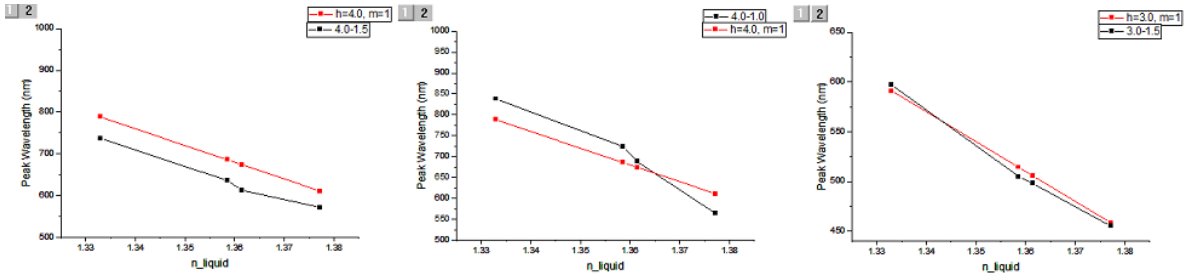

Figure 17: MATLab Simulations (Red) Plotted Against Experimental Data (Black) For Samples in Liquid (4.0-1.5, 4.0-1.0, and 3.0-1.5)

Figure 17 shows the predicted peak wavelengths of samples 4.0-1.5, 4.0-1.0, and 3.0-1.5 (height-gap) in water, acetone, ethanol, and IPA (red) as well as the experimental data (black).

For samples 4.0-1.5, 4.0-1.0, and 3.0-1.5, the experimental data also follows the MATLAB simulation trend. Although (in the case of 4.0-1.0 and 3.0-1.5), the simulated data crosses

over the experimental data, and in the case of 4.0-2.0 the simulated data lies solely above the simulated data, the increase in peak wavelength with decrease of refractive index holds true for all cases (and all other experimental data obtained for this report), and thus follows the MATLAB trend (as well as the blueshift results from the previous section) as expected. Finally, MATLab simulations were performed for expected peak wavelength as a function of structure height. Due to the position of the 1.5 to 2.0 micrometre structure first order peaks lying below 400 nm (where the data was cut off when smoothed), only structures with heights from 2.5 to 4.0 micrometres were included in this analysis. The peak wavelength was found to decrease as refractive index and gap width increased. Since a peak wavelength increase of 152 nm (h=2.5 micrometres) and 34 nm (h=4.0 micrometres) occurred for water as the gap increased by 1.5 micrometres, whereas a peak wavelength increase of 93 nm (h=2.5 micrometres) and 51 nm (h=4.0 micrometres) occurred for a gap of 2.5 micrometres for samples in water and acetone (with a corresponding refractive index increase of 0.026, one can assume that the change in gap width results in a higher peak wavelength difference than the change in refractive index.

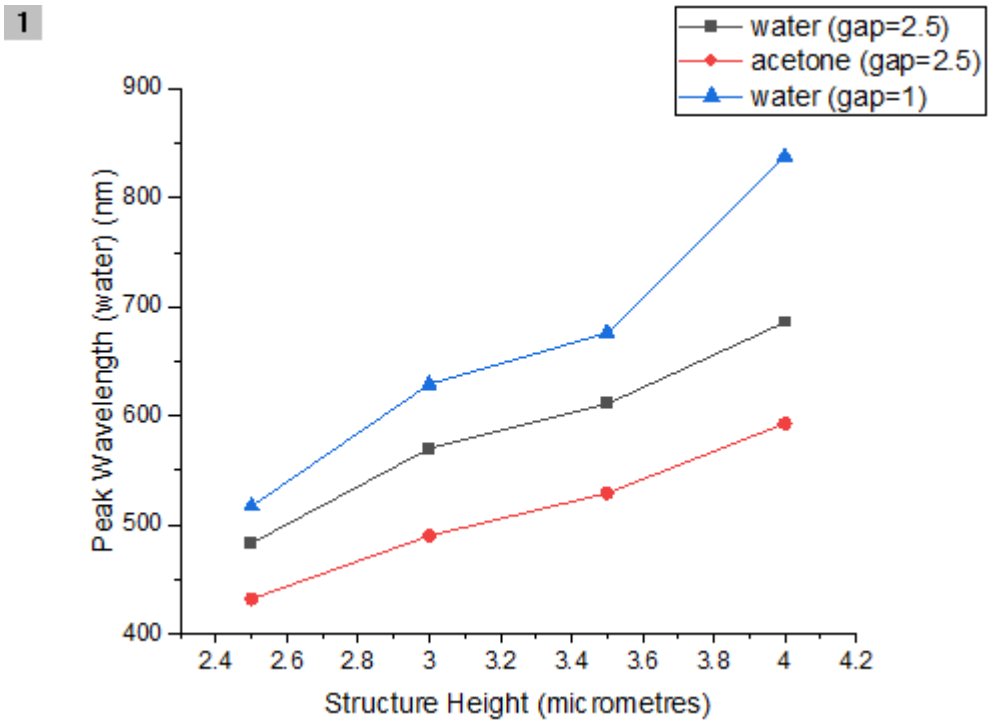

Figure 18: Experimental Data of Samples with Gap Width 2.5 and 1.0 Micrometres in Water and Acetone

Figure 18 shows the experimental data which led to the analysis of the significance of refractive index change as opposed to the significance of structure gap width change. In this

case, the term significance is intended to convey the difference in peak wavelength when corresponding parameters are changed.

Since peak wavelength (Equation 1) is directly proportional to structure height, one may conclude that as structure height increases, expected peak wavelength will also increase. This is proven by a plot of peak wavelength as a function of structure height for all columns of samples in all liquids used.

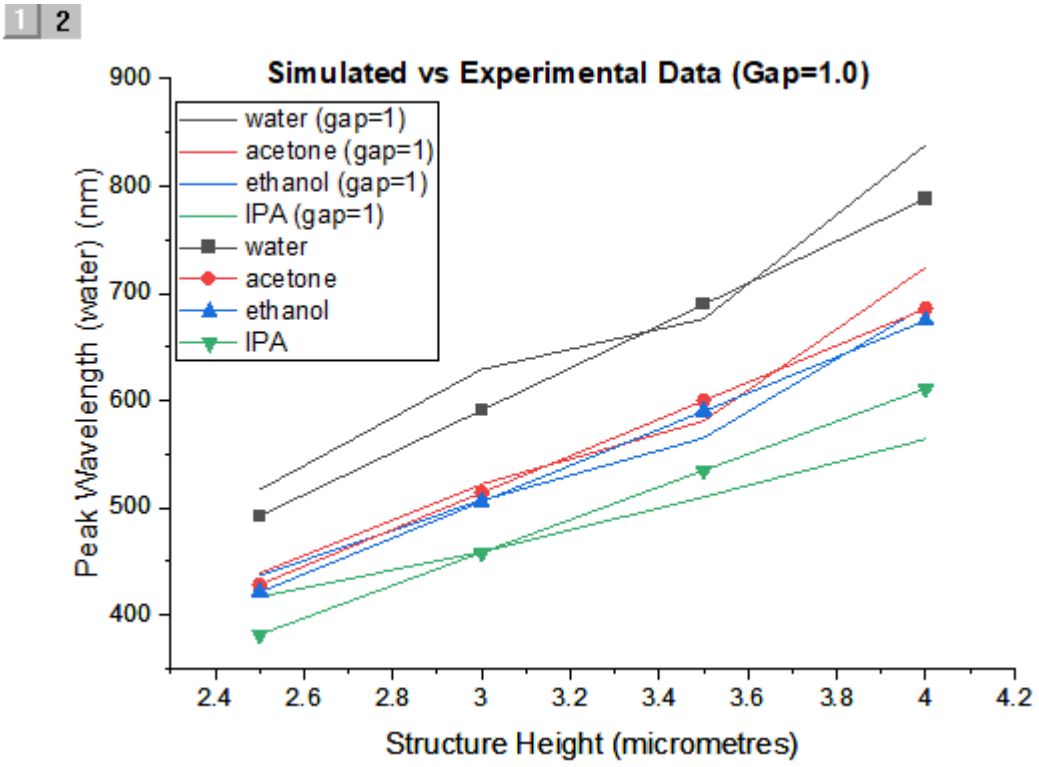

Figure 19: Simulated (MATLAB) vs Experimental Data for Samples with a Gap Width of 1.0 Micrometres

Figure 19 shows simulated data (line and symbol plots) with experimental data (line plots) for samples with heights ranging from 2.5 to 4 micrometres. The four sets of plots correspond to samples in water, acetone, ethanol, and IPA.

As predicted from Equation 1 and the MATLAB model, the experimental data shows that peak wavelength increases with structure height. This shift from low to high wavelength can be classified as a redshift (as opposed to a shift from high to low wavelength which is referred to as a blueshift) as structure height increases.

Conclusions: At the zeroth order, visually analysing contour plots of structure height as a function of wavelength led to the observation that the phase grating equation most closely matched experimental data when the aspect ratio was 0.25. A previous experimental analysis of transmission phase theory[1] used Kirchhoff's scalar wave theory to produce a zero-order

diffraction efficiency equation which predicted the most vibrant colours for structures with an aspect ratio of 0.5, but the results obtained found the expected results at an aspect ratio of approximately 0.3. Using chromaticity diagrams, the most vibrant colours were identified as those with an aspect ratio of 0.33. These results led to the conclusion that although structures with an 0.33 aspect ratio have the most vibrant colours, structures with an 0.25 aspect ratio most closely adhere to phase grating theory (such that the saturation of the samples is greatest with an 0.33 aspect ratio but the correlation of the peaks with respect to theory is greatest with an 0.25 aspect ratio from the samples analysed). The sample from the column with an 0.33 aspect ratio which possessed the greatest saturation at high angles (20-25 degrees) was sample 1.5-1.5 (height-gap in microns) from slide 2. The order of the expected intensity at wavelengths in the visible spectrum from Lumerical simulations agreed with experimental data approximately 71 % of the time (if error bars are assumed to convey the expected result when possible) for angles 0, 10, and 20 degrees. The expected blueshift for samples in water, acetone, ethanol, and IPA occurred for all structures as the refractive indices of the liquids increased which gave rise to the proposition of usefulness of such samples in colorimetric sensing; specifically to identify the refractive index of liquids using the diffracted peak location compared to that of the sample in other liquids of known refractive index. Using Equation 1, MATLAB models, and experimental data (all of which conveyed the same trend), it was concluded that a structure height increase produced an increase in peak wavelength (redshift) for a given structure in liquid. The MATLAB models and experimental data suggest potential use of IPL grating samples as colorimetric sensors. The high saturation of samples at the zeroth order may be used to introduce structural colour to industries such as fashion or technology as an eco-friendly alternative to dye. If structures are found with dimensions which produce low saturation at low angles and high saturation at greater angles (or vary by angle in another form which would be difficult to replicate), this could be used on items such as IDs to ensure a simple (purely visual) way to identify an illegally manufactured item.

Bibliography

[1] K. Knop, "Rigorous diffraction theory for transmission phase gratings with deep rectangular grooves," J. Opt. Soc. Am. 68, 1206-1210 (1978)

[2] Liu, Y., Wang, H., Ho, J. et al. Structural color three-dimensional printing by shrinking photonic crystals. Nat Commun 10, 4340 (2019). https://doi.org/10.1038/s41467-019-12360-w

[3] Gordon Zyla, Alexander Kovalev, Silas Heisterkamp, Cemal Esen, Evgeny L. Gurevich, Stanislav Gorb, and Andreas Ostendorf, "Biomimetic structural coloration with tunable degree of angle-independence generated by two-photon polymerization," Opt. Mater. Express 9, 2630-2639 (2019)

[4] Lenau, T. A. (2012). Nature inspired structural colour applications. In O. Karthaus (Ed.), Biomimetics in Photonics (pp. 72-96). CRC Press. Series in Optics and optoelectronics

[5] **Polym. Chem.**, 2017,**8**, 10-11

[6] APL Photonics 4, 070402 (2019); https://doi.org/10.1063/1.5115150

[7] Zhang, W., Wang, H., Wang, H. et al. Structural multi-colour invisible inks with submicron 4D printing of shape memory polymers. Nat Commun 12, 112 (2021). https://doi.org/10.1038/s41467-020-20300-2

[8] J. Mater. Vje,. C. 2021, 9, 11674

[9] Hua Gao, Min Ouyang, Yu Wang, Yan Shen, Jing Zhou, Dahe Liu. Analysis on diffraction properties of the transmission phase grating. Optik, Volume 118, Issue 9, 2007, Pages 452-456, ISSN 0030-4026, https://doi.org/10.1016/j.ijleo.2006.04.017.

[10] Michał Nawrot, Łukasz Zinkiewicz, Bartłomiej Włodarczyk, and Piotr Wasylczyk, "Transmission phase gratings fabricated with direct laser writing as color filters in the visible," Opt. Express 21, 31919-31924 (2013)

[11] Pelant, Ivan, and Jan Valenta, 'Photonic structures', Luminescence Spectroscopy of Semiconductors (Oxford, 2012; online edn, Oxford Academic, 24 May 2012), https://doi.org/10.1093/acprof:oso/9780199588336.003.0016

[12] Britannica, T. Editors of Encyclopaedia (2016, October 26). diffraction grating. Encyclopedia Britannica. https://www.britannica.com/technology/diffraction-grating

[13] *Diffraction and Interference of Light.* (2019). University of Texas at San Antonio. https://www.utsa.edu/physics/resources/lab-1631/Diffraction.pdf

[14] Polym. Chem., 2017, **8**, 127-143

[15] Faraji Rad, Z., Prewett, P.D. & Davies, G.J. High-resolution two-photon polymerization: the most versatile technique for the fabrication of microneedle arrays. Microsyst Nanoeng **7**, 71 (2021). https://doi.org/10.1038/s41378-021-00298-3

[16] Pike, R. A. (2022, April 25). adhesive. Encyclopedia Britannica. https://www.britannica.com/technology/adhesive

[17] *Sensors* **2013**, *13*(4), 4192-4213; **https://doi.org/10.3390/s130404192**

[18] Volk, János & Grand, T & Bársony, I. & Gombkötő, J & Ramsden, Jeremy. (2005). Porous silicon multilayer stack for sensitive refractive index determination of pure solvents. Journal of Physics D: Applied Physics. 38. 1313. 10.1088/0022-3727/38/8/032.

[19] Britannica, T. Editors of Encyclopaedia (2019, December 23). refractive index. Encyclopedia Britannica. https://www.britannica.com/science/refractive-index

Appendix

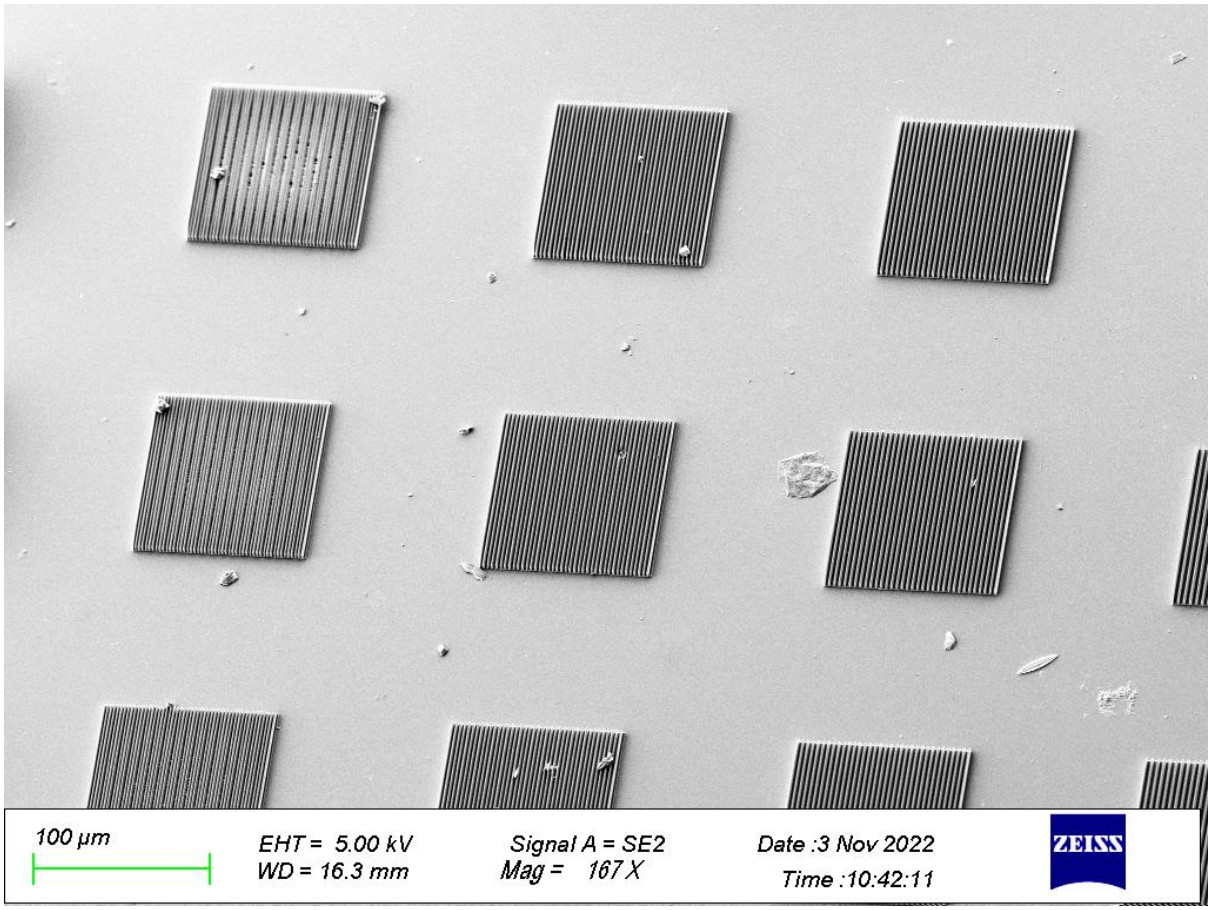

SEM Image of Slide 1

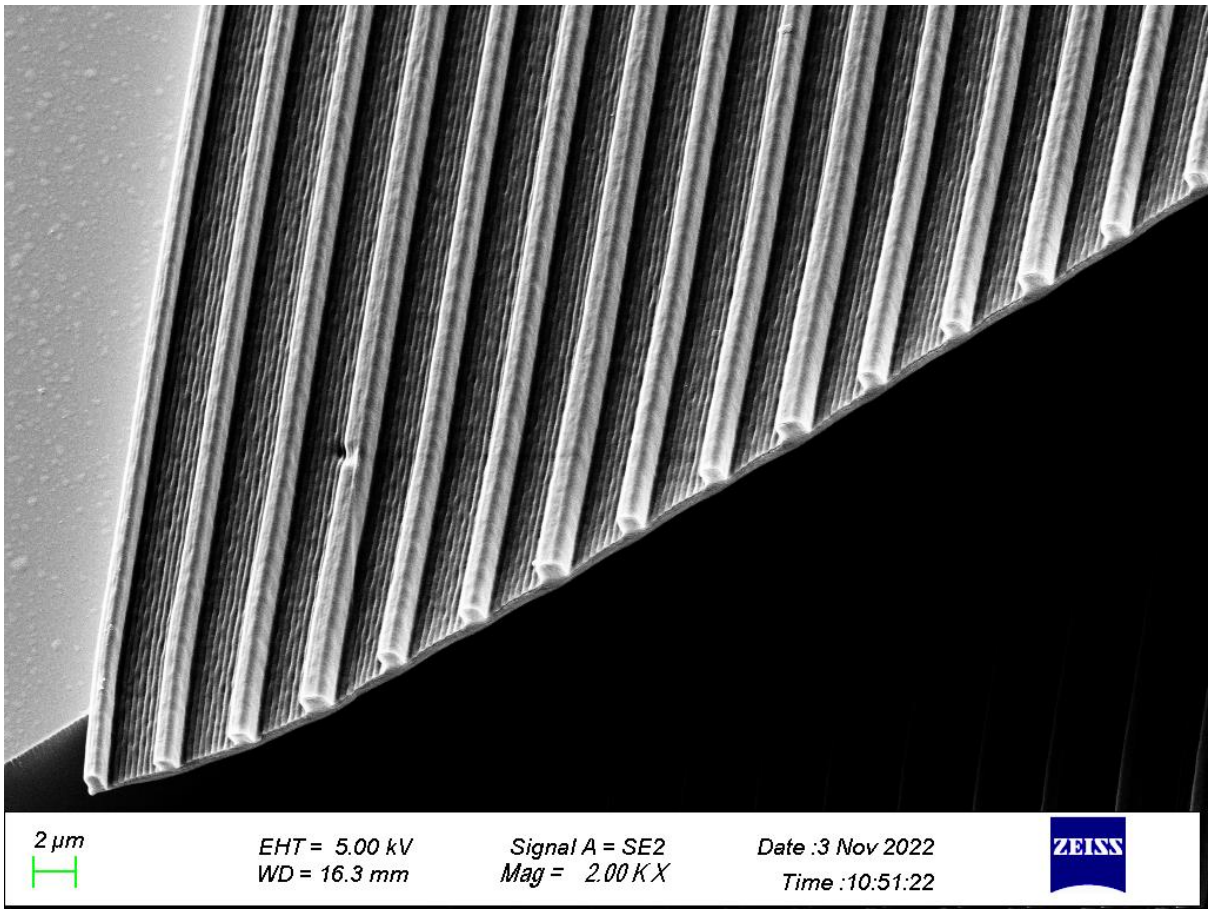

SEM Image of Slide 1 Sample 1.5-2.5 (Broken)

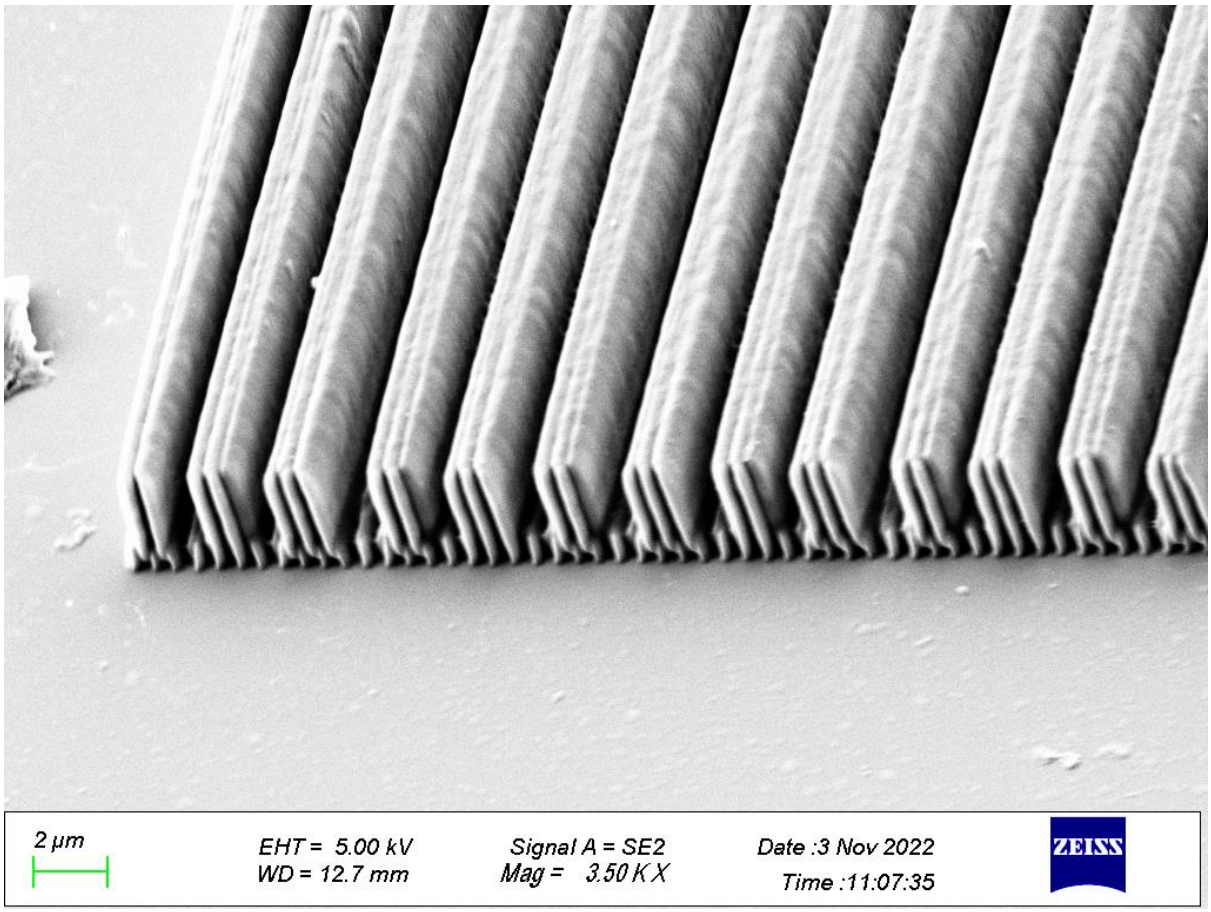

SEM Image of Slide 1 Sample 4.0-2.5

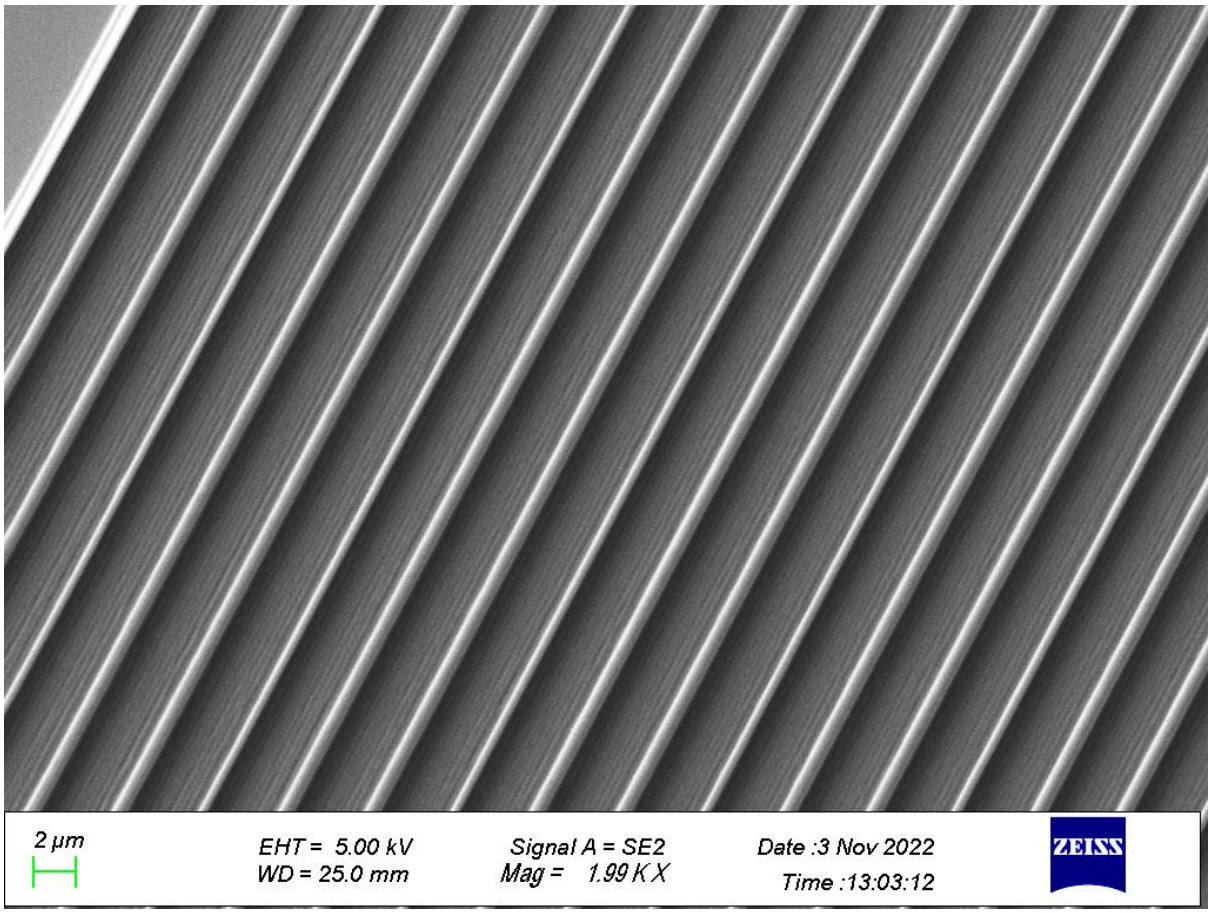

SEM Image of Slide 2 Sample 2.0-3.0